Optical properties and device characteristics of 2-(antipyrin4-ylhydrazono)-2-(4-nitrophenyl)acetonitrile thin films for photodiode applications

ARTICLE *in* SPECTROCHIMICA ACTA PART A MOLECULAR AND BIOMOLECULAR SPECTROSCOPY · SEPTEMBER 2014

Impact Factor: 2.35 · DOI: 10.1016/j.saa.2014.09.006 · Source: PubMed

2 AUTHORS:

Emad El-Menyawy
National Research Center (CO, USA)
27 PUBLICATIONS **195** CITATIONS
SEE PROFILE

Islam Zedan
H.I.E.T. El-Arish
17 PUBLICATIONS **64** CITATIONS
SEE PROFILE

Spectrochimica Acta Part A: Molecular and Biomolecular Spectroscopy 137 (2015) 810–816

Contents lists available at ScienceDirect

Spectrochimica Acta Part A: Molecular and Biomolecular Spectroscopy

journal homepage: www.elsevier.com/locate/saa

Optical properties and device characteristics of 2-(antipyrin-4-ylhydrazono)-2-(4-nitrophenyl)acetonitrile thin films for photodiode applications

E.M. El-Menyawy [a,*], I.T. Zedan [b]

[a] Solid State Electronics Laboratory, Solid State Physics Department, Physics Division, National Research Center, Dokki, Cairo 12311, Egypt
[b] Basic Science Department, High Institute of Engineering and Technology, El-Arish, North Sinai, Egypt

HIGHLIGHTS

- Optical properties of an antipyrine derivative were studied.
- The film deposited on n-silicon substrate showed good rectification behaviour.
- The ideality factor and barrier height of the device were obtained to be 2.62 and 0.74 eV, respectively.
- The fabricated diode can be used for optical sensor applications.

GRAPHICAL ABSTRACT

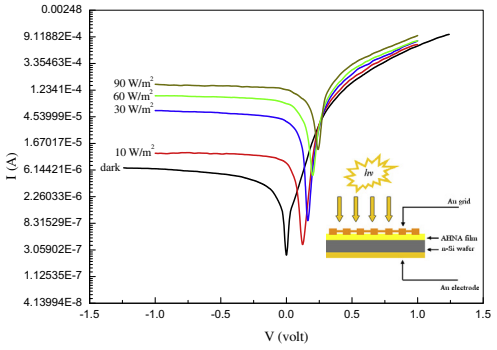

ARTICLE INFO

Article history:
Received 20 May 2014
Received in revised form 2 September 2014
Accepted 3 September 2014
Available online 16 September 2014

Keywords:
Antipyrines
Optical properties
Heterojunctions
Electrical characterisation
Photodiode

ABSTRACT

2-(Antipyrin-4-ylhydrazono)-2-(4-nitrophenyl)acetonitrile (AHNA) films were deposited via thermal evaporation technique. The optical properties of AHNA films and electrical characteristics of Au/AHNA/n-Si/Au heterojunction diode have been reported. The optical properties of AHNA films were investigated using the spectrophotometric measurements of optical transmittance and reflectance over spectral range 190–2500 nm. The films have indirect allowed optical band gap of 3.6 eV. The refractive index of the films was calculated and the dispersion parameters of the films were determined on the light of the single oscillator model. The electrical properties of Au/AHNA/n-Si/Au heterojunction diode were studied in terms of current–voltage characteristics. The device showed rectification behaviour with a rectification ratio of 100 at ±1 V. The conduction mechanisms and diode parameters such as ideality factor, barrier height and series resistance of the device were determined. The device under illumination showed photovoltaic properties. The short circuit current and open circuit voltage were found to be function of illumination intensity. The device satisfies the conditions to be used as photodiode.

Introduction

Organic materials have been extensively investigated and used in the fields of electronic and optoelectronic devices due to the possibility of optoelectronic features and the possibility of producing large area devices of these materials. They have been used for producing high performance light emitting diodes (LEDs) [1,2], thin-film transistors (TFTs) [3,4], and photovoltaic cells (PVCs) [5,6]. The performance of these devices is significantly depending on the electronic structure of the interfaces within the devices. In organic LEDs and TFTs, charges must be injected from electrodes

* Corresponding author. Tel.: +20 1006021326; fax: +20 233709310.
E-mail address: emad_elmenyawy@yahoo.com (E.M. El-Menyawy).

http://dx.doi.org/10.1016/j.saa.2014.09.006
1386-1425/

into the organic semiconductor, which requires that energy barriers for charge injection must be minimised to achieve low operation voltages. In organic PVCs, the contact between an electron acceptor and electron donor materials represents the most important element because that the exciton dissociation occurs with high probability.

Metal/organic/inorganic semiconductor devices have been investigated and showed modification in barrier properties [7] and good rectification behaviour [8]. These devices have some advantages like easy fabrication and can be used as a photodiode in photovoltaic applications [9–11]. The current–voltage (I–V) characteristics of organic/inorganic (OI) devices are controlled by the charge injection at the OI interface and by the electrical transport in bulk material. The characteristic parameters of such devices are controlled by the case OI interface which can be reflected on the values of two important parameters namely the ideality factor and barrier height. The series resistance is an important parameter for controlling the performance of these devices through affecting the charge carriers' transport.

The junction properties were found to depend on the organic material itself. This inspires the researchers to search for new organic materials. Antipyrines derivatives are a class of organic compounds that have been studied extensively due to their fascinating properties. In recent research papers, El-Menyawy et al. reported on the synthesis and characterisation of some antipyrine derivatives [12–17] for electronic and optoelectronic applications. It is found that antipyrine derivatives have been used for solar cells applications [14,15]. More recently, it is found that antipyrine derivatives can be used for Schottky junction fabrication [17]. In view of the considerable importance of these compounds, we are thus interested in extending these studies to design and make materials with potential technological applications. The title compound, 2-(antipyrin-4-ylhydrazono)-2-(4-nitrophenyl)acetonitrile (AHNA), with its molecular structure shown in scheme 1 has been recently synthesised and electrically investigated by us for the first time [18]. The study showed that the AHNA exhibits semiconductor behaviour. In this work, we report on the optical properties of AHNA films. Additionally, the electrical and photoelectrical proprieties of Au/AHNA/n-Si/Au heterojunction diode were studied.

Experimental

Si wafer (doped with phosphorus) substrates with (1 0 0) orientation, 0.4 mm thickness and 1–10 Ω cm resistivity were used for device manufacturing. The n-Si wafer was chemically cleaned by using the well known RCA cleaning procedure (10 min boil in $NH_3 + H_2O_2 + 6H_2O$ followed by a 10 min heating in $HCl + H_2O_2 + 6$-H_2O at 60 °C). The native oxide on the n-Si substrate was removed in $HF + 10H_2O$ solution. Then, the ohmic contact was made by depositing gold films on the back surface of the Si substrate. The wafer-coated gold film was annealed at 450 °C for 5 min in argon atmosphere. After that, AHNA films were deposited on the front surface of Si wafer. The thickness of the organic layer was determined as 120 nm. Finally, gold electrode contact was fabricated on the organic layer by using shadow mask made from aluminium foil. Scheme 2 shows the schematic diagram of the manufactured Au/AHNA/n-Si/Au heterojunction. The cross-section are of the diode was 0.2 cm^2.

The AHNA powder used for preparing thin films was synthesised by us elsewhere [18]. AHNA and Au films were deposited onto substrates, maintained at room temperature, by using conventional thermal evaporation technique. The high-vacuum evaporation unit (Edwards 306 A) was used to deposit the films under base pressure of 8×10^{-6} Torr. AHNA was evaporated under vacuum by using a quartz crucible that was subjected to induction heating by using tungsten filament lamp.

In order to study the optical properties of AHNA films, optical flat fused quartz substrates were used. The absorption coefficient and the refractive index were investigated as a function of wavelength. For this purpose, the optical transmittance and reflectance were measured at normal incidence of the light over the spectral range 190–2500 nm. The transmittance and reflectance spectra of the films were recorded by means of a double beam spectrophotometer (JASCO model V-570 UV–vis-NIR). The measurements were achieved at room temperature. The optical functions were calculated from the absolute values of total measured transmittance (T_m) and reflectance (R_m) after introducing corrections resulting from the absorbance and reflectance of the substrate. The absolute value of T_m was computed by [19]:

$$T = T_m(1 - R_q) \quad (1)$$

and the absolute value of R_m was computed by:

$$R = R_m R_{Al}\left[(1 - R_q)^2 + 1\right] - T^2 R_q \quad (2)$$

where R_q and R_{Al} are the reflectance of reference quartz substrate and that of the reference aluminium mirror, respectively.

The current–voltage characteristics of Au/AHNA/n-Si/Au heterojunction were recorded under darkness and illumination conditions using Keithley 2635 A source-meter. The temperature of the sample was recorded during the measurements by using NiCr–NiAl thermocouple connected to digital thermometer. The incident power flux was recorded by a calibrated Lux-meter.

Results and discussion

Optical properties

AHNA thin films were characterised through spectral transmittance and reflectance measurements, in order to determine the absorption coefficient and refractive index. The spectral

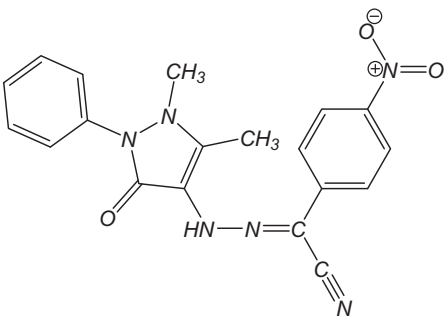

Scheme 1. The molecular structure of AHNA compound.

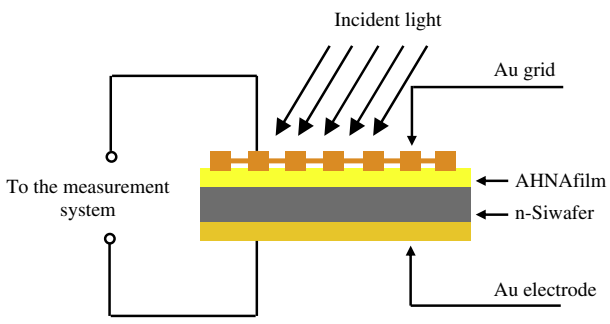

Scheme 2. Schematic diagram showing Au/AHNA/n-Si/Au heterojunction diode.

distribution of the optical transmittance and reflectance for AHNA film of thickness 120 nm is demonstrated in Fig. 1. The transmittance of the films is very low at wavelengths below 300 nm, and then it increases rapidly up to 400 nm showing a fundamental transmittance edge. The films show another edge over the spectral range 460–580 nm. Above this value the transmittance increases slightly with increasing the wavelength. The reflectance of the films shows two peaks at wavelength values of 360 and 480 nm. Above this value, the reflectance of the films decreases slightly with increasing wavelength and saturates at higher wavelengths. As general observation, at wavelengths less than 560 nm, the films are absorbing, whereas at wavelengths greater than this value the films are transparent.

The absorption coefficient of optical materials is of great importance in which it describes the absorption process in different photon energy regions. It can be used for determining the nature of electronic inter-band transitions and evaluating the optical band gap on nonmetallic materials. The absorption coefficient (α) of the films was calculated in terms the absolute values of the transmittance and reflectance using the expression given by [20]:

$$\alpha = \frac{1}{d}\ln\left[\frac{(1-R)^2}{2T} + \sqrt{\frac{(1-R)^4}{4T^2} + R^2}\right] \quad (3)$$

where d is the film thickness. The spectral distribution of the absorption coefficient for the films is represented in Fig. 2. At low photon energies less than 2.2 eV, the absorption has low values. Above this value, the absorption coefficient increases slightly with increasing photon energy before starting to increase rapidly showing high intense four absorption peaks located at 4.43, 4.77, 5.39 and 5.91 eV. The absorption edge can be used to determine the optical band gaps of the films using Tauc's expression given by [21]:

$$\alpha = \frac{G}{h\nu}(h\nu - E_g)^s \quad (4)$$

where G is a parameter depending on transition probability and E_g is the optical band gap. In this equation, the exponent s takes the value 1/2 for direct allowed optical transitions, and 3/2 for the direct forbidden ones. In addition, it takes the value 2 for indirect allowed optical transitions and 2/3 for the indirect forbidden ones. The optical band gap value can be obtained from the best linear approximation in the $(\alpha h\nu)^{1/s}$ versus $h\nu$ plot and its extrapolation to $(\alpha h\nu)^{1/s} = 0$. The best fitting for the films under investigation is obtained for $s = 2$ indicating that the electronic transition is through indirect allowed process. Tauc's plot for obtaining the optical band

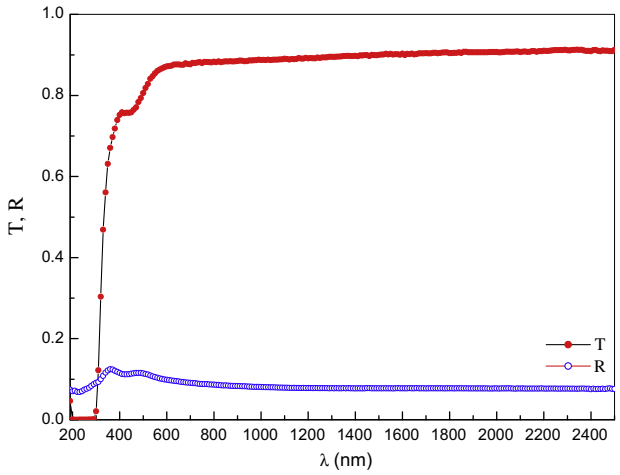

Fig. 1. The spectral behaviour of transmittance and reflectance measured at normal incidence of light.

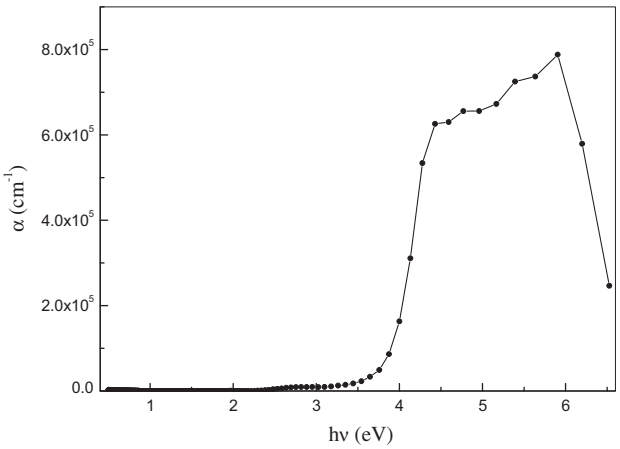

Fig. 2. Absorption coefficient spectra of AHNA films.

gap of the films is depicted in Fig. 3. The fundamental optical band gap of the films is estimated as 3.60 eV.

Below the optical band gap, the absorption coefficient shows exponential behaviour. This behaviour indicates that there are defects or impurities causing the band structure of the films to perturb resulting in a prolonged tail extending into the energy gap. The exponential behaviour of the absorption coefficient follows Urbach's empirical relation [22]:

$$\alpha = \alpha_o \exp\left(\frac{h\nu}{E_U}\right) \quad (5)$$

where α_o is a parameter depending on the material and E_U is the Urbach energy width of the exponential tail. The relation between the natural logarithm of the absorption coefficient and photon

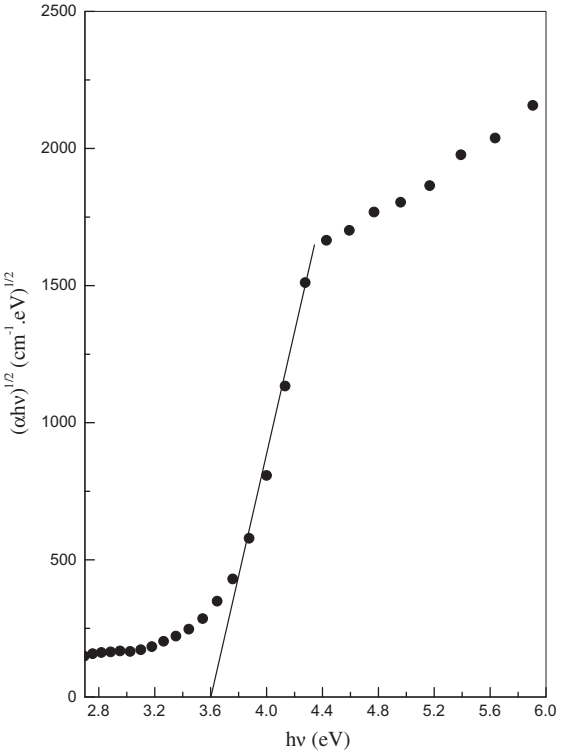

Fig. 3. Tauc's plot of AHNA films showing the determination of the indirect allowed optical band gap.

energy is shown in Fig. 4. The relation is linear and the value of E_U is determined as 0.48 eV from the slope of the straight line.

The refractive index of optical materials is greatly importance for the electronic and optoelectronic applications in which the refractive index plays a vital role in devices design. The refractive index of the films is calculated by the equation [23]:

$$n = \frac{1+R}{1-R} + \sqrt{\frac{4R}{(1-R)^2} - k^2} \quad (6)$$

where k is the absorption index of the films which is calculated using the well known relation; $k = \alpha\lambda/4\pi$. The dispersion curve of the refractive index for AHNA films is illustrated in Fig. 5. As can be observed, the anomalous dispersion exists in the wavelength range 190–560 nm, in which the refractive index exhibits five peaks located at 210, 230, 280, 360 and 480 nm. This behaviour can be explained according to multi-oscillator model [24]. At wavelengths greater than 560 nm, the refractive index of the films decreases with increasing wavelength and saturates at high wavelengths. This behaviour is the normal dispersion and can be explained by the single oscillator model. The experimental data of the refractive index was analysed by using the single oscillator model developed by Wemple and DiDomenico [25]. In terms of this model, the normal dispersion of the refractive index can be described, to a very good approximation by the following relation:

$$n^2 = 1 + \frac{E_d E_o}{E_o^2 - (h\nu)^2} \quad (7)$$

where E_d is the dispersion energy and E_o is the energy of the effective dispersion oscillator. According to this equation, the relation between $(n^2-1)^{-1}$ and $(h\nu)^2$ is linear, in which the oscillator parameters can be determined from the intercept (E_o/E_d) and the slope $(1/E_oE_d)$. Fig. 6 represents the relation between $(n^2-1)^{-1}$ and $(h\nu)^2$ for AHNA films. The relation is linear verifying Eq. (7), from which the values of E_d and E_o are estimated as 8.57 and 4.22 eV, respectively. In addition, by extrapolating the linear part towards zero photon energy, the interception on $(n_\infty^2-1)^{-1}$ axis can be used for the determination of the optical dielectric constant $(\varepsilon_\infty = n_\infty^2)$ which is estimated as 3.03.

Current–voltage characteristics

Fig. 7 illustrates the semilogarithmic current–voltage (I–V) characteristics of Au/AHNA/n-Si/Au heterojunction diode measured in dark at room temperature. The forwarded current increases exponentially up to 0.34 V, and then shows a curvature

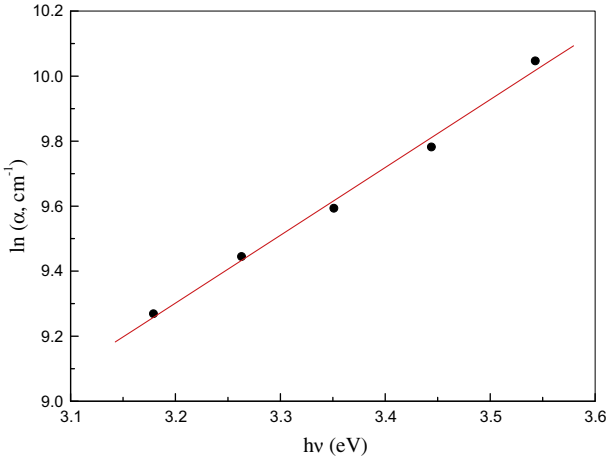

Fig. 4. Urbach's relation of AHNA films.

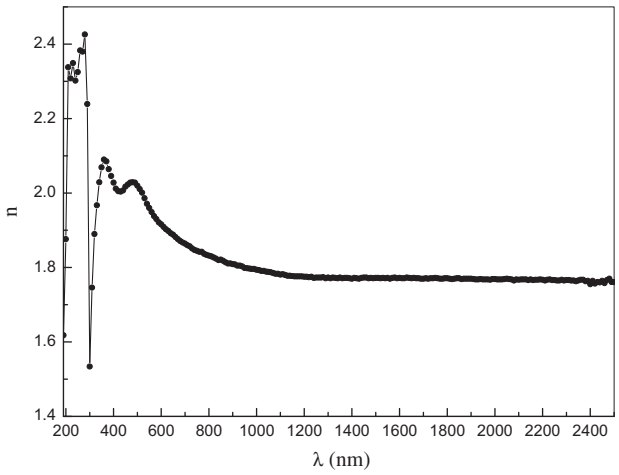

Fig. 5. The spectral distribution of the refractive index for AHNA films.

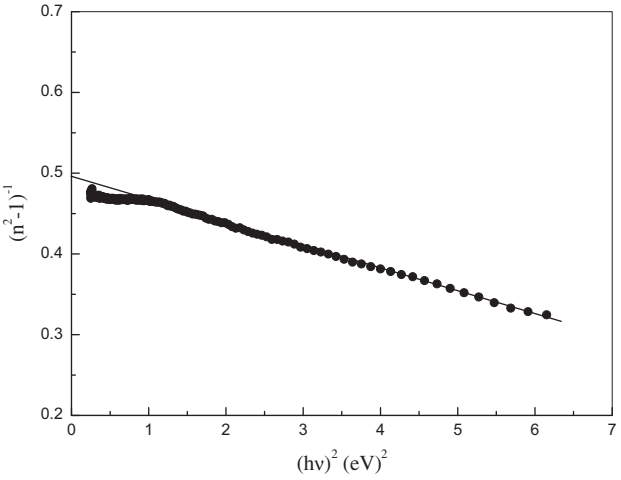

Fig. 6. The relation between $(n^2-1)^{-1}$ and squar photon energy of AHNA films.

with further increase in applied voltage. In reverse bias direction, the current shows saturation. Such trend is responsible for good rectification behaviour. The rectification ratio has a factor of 100 achieved between the forward and reverse bias current at ±1 V, and the diode has reverse saturation current of 8.69×10^{-7} A. The linear behaviour of the semilogarithmic I–V plot at low applied voltage indicates that the current of the device could be expressed by the standard diode equation [26]:

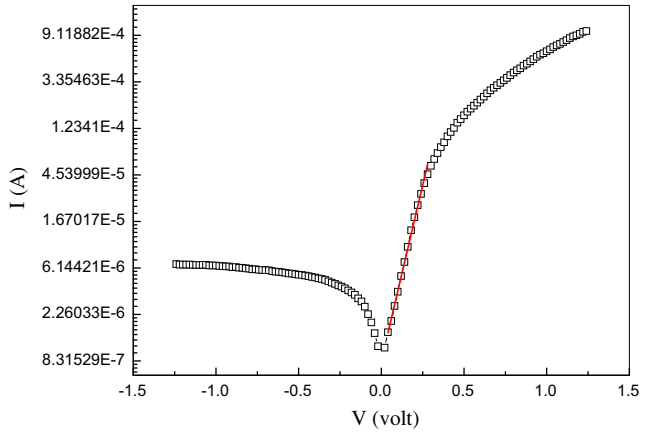

Fig. 7. The semilogarithmic I–V characteristics of Au/AHNA/n-Si/Au heterojunction.

$$I = I_s\left[\exp\left(\frac{eV}{mk_BT}\right) - 1\right] \tag{8}$$

with

$$I_s = AA^*T^2 \exp\left(\frac{e\phi}{k_BT}\right) \tag{9}$$

where I_s is the saturation current, e is the electronic charge, V is the applied voltage, m is the dimensionless diode ideality factor, k_B is the Boltzmann constant, T is the absolute temperature, A is the diode area, A^* is the effective Richardson constant and ϕ is the zero-bias barrier height.

The ideality factor of the diode was determined as 2.62 by using Eq. (8). The obtained ideality factor is higher than unity, indicating that the diode exhibits a non-ideal behaviour which can be attributed to several reasons such as large surface leakage current, high density of bulk recombination centers in the depletion region, and high interface state density as well as high series resistance [27]. By substituting the value of A^* as 112 A cm^{-1} K^{-2} [28] in Eq. (9), the value of zero-bias barrier height for the device is estimated as 0.74 eV. The value of ϕ is higher than that of conventional Au/n-Si diode (0.668) [29] and is comparable with similar Au/organic/n-Si diodes [30–32].

The high value of the ideality factor and the downward concave curvature of the forward bias I–V plot at high applied voltage indicate that the series resistance effect plays important role in determining the performance of the device. Norde proposed a method to estimate the series resistance and barrier height of diodes. Norde's function can be expressed as [33]:

$$F(V) = \frac{V}{\gamma} - \frac{k_BT}{e}\ln\left(\frac{I(V)}{AA^*T^2}\right) \tag{10}$$

where γ is the first integer greater than the value of m and $I(V)$ is current obtained from the I–V curve. The series resistance of the device is determined by using the relation given by:

$$R_s = \left(\frac{k_BT}{e}\right)\left(\frac{\gamma - m}{I(V_{min})}\right) \tag{11}$$

where $I(V_{min})$ is the current corresponding to the voltage that has a minimum point of $F(V)$. The barrier height is deduced from the expression given by:

$$\phi = F(V_{min}) + \frac{V_{min}}{\gamma} - \frac{kT}{e} \tag{12}$$

where $F(V_{min})$ is the minimum point of $F(V)$ and V_{min} is the corresponding voltage. Fig. 8 illustrates the relation between $F(V)$ and the forward applied voltage. The relation shows minimum value of $F(V)$ at applied voltage of 0.22 eV. The series resistance and barrier height of the device were estimated as 415 Ω and 0.77 eV, respectively.

For further analysis, the contribution of higher forward applied voltages to I–V characteristics of the device is investigated by plotting the I–V characteristic on double natural logarithmic scale as shown in Fig. 9. The relation shows a straight line with a slope of 2.02. This result indicates that the mechanism of conduction is the space charge limited current dominated by single trap [34]. This suggests that the conduction process of AHNA film makes a contribution to the I–V characteristics of the diode.

At reverse biasing, the current of the device is low compared with the forward one suggesting that the current in reverse direction can be governed by current limitation mechanism. The relation between the natural logarithm of the leakage current and the root mean square of the voltage is depicted in Fig. 10. The relation could be analysed in terms of two field lowering mechanisms namely Schottky (Sc) and Poole–Frenkel (PF) mechanisms [35].

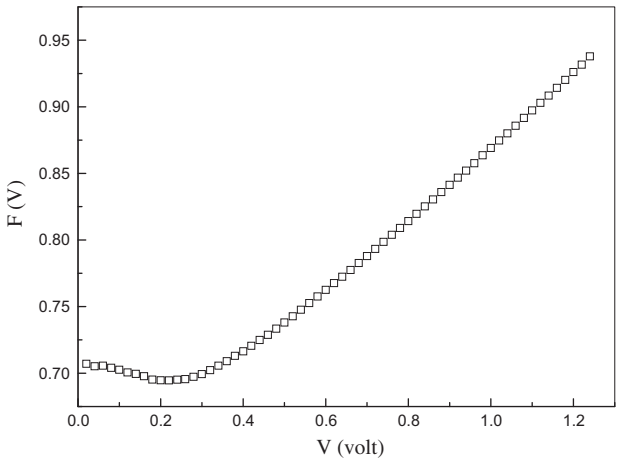

Fig. 8. Norde's function as a function of forward applied voltage for Au/AHNA/n-Si/Au heterojunction.

For Sc mechanism, the current is given by:

$$I = AA^*T^2 \exp\left[\left(\frac{\beta_{Sc}V^{1/2}}{d^{1/2}} - \phi_{Sc}\right)\Big/ k_BT\right] \tag{13}$$

For PF mechanism, the current is given by:

$$I = I_s \exp\left(\frac{\beta_{PF}V^{1/2}}{k_BTd^{1/2}}\right) \tag{14}$$

where ϕ_{Sc} is the barrier height for Schottky mechanism and d is the film thickness. The parameters β_{PF} and β_{Sc} are the field-lowering coefficients for PF and Sc mechanisms, respectively.

The theoretical values for both β_{PF} and β_{Sc} are given by the following well-known relation,

$$\beta_{PF} = 2\beta_{Sc} = \left(\frac{e^3}{\pi\varepsilon\varepsilon_o}\right)^{1/2} \tag{15}$$

Using the value of ε determined from the optical study, the theoretical values of β_{PF} and β_{Sc} were calculated as 4.36×10^{-5} and 2.18×10^{-5} eV m$^{1/2}$ V$^{1/2}$, respectively. The values of field-lowering coefficients in the low-voltage and high voltage regions were estimated as 4.28×10^{-5} and 0.70×10^{-5} eV m$^{1/2}$ V$^{1/2}$, respectively. The experimentally calculated value at low voltage region is comparable with the theoretical values of β_{PF} and is 0.32 times the value for the theoretical value of β_{Sc}. The difference between the theoretical and experimental value of β_{Sc} at higher voltage region

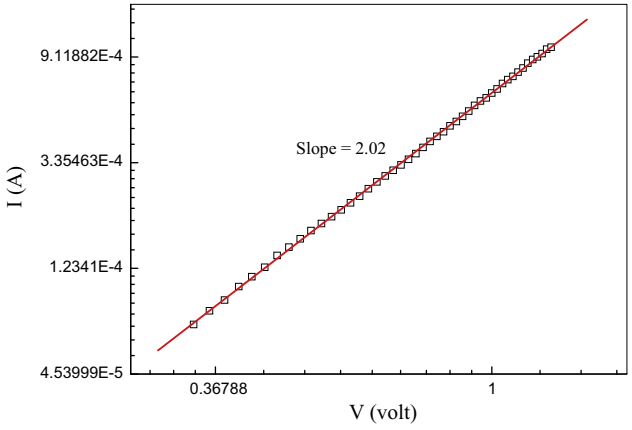

Fig. 9. Double natural logarithmic I–V characteristics at voltages greater than 0.34 V.

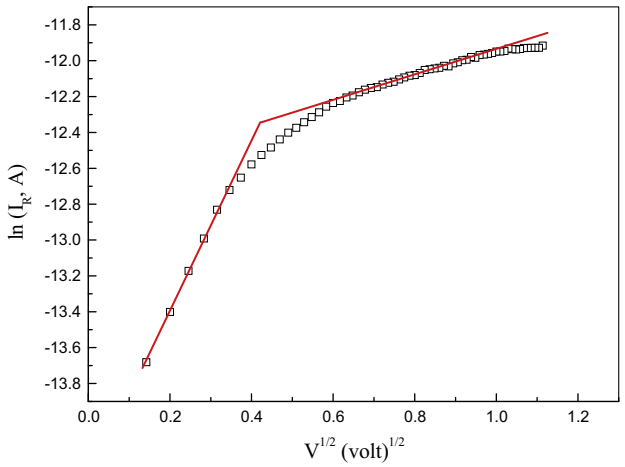

Fig. 10. The variation of the natural logarithm of the reverse current with the square root of the applied voltage.

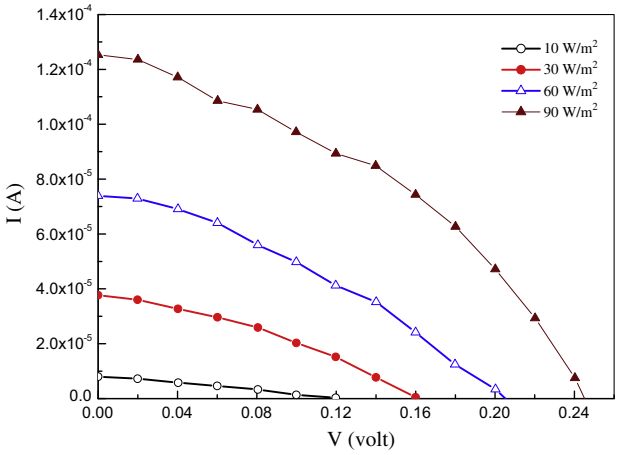

Fig. 12. The power curve of Au/AHNA/n-Si/Au heterojunction diode under different illuminations.

can be due to thermally assisted tunnelling field emission of carriers across thin barriers [36] or can be explained in terms of a Schottky depletion region extending only in a short distance and not across the entire Si layer [37]. This suggests that Poole–Frenkel emission is dominant in the lower voltage region whereas Schottky emission is dominant in the higher voltage region.

The current–voltage characteristics of the Au/AHNA/n-Si/Au heterojunction diode under various illumination intensities are depicted in Fig. 11 (the dark curve is inserted for comparison). With increasing light intensity, the current in reverse bias increases strongly due to the generation of carrier charges. In forward direction, the device delivered an open circuit voltage (V_{oc}) along with a short circuit current (I_{sc}). Fig. 12 shows the power curve obtained at various illumination intensities. The photoresponsivity (I_{light}/I_{dark}), short circuit current and open circuit voltage at various illumination intensities are listed in Table 1. With increasing light intensity, the photovoltaic parameters are improved. The increased reverse current and the obtained photovoltaic values are typical values for optoelectronic applications as they satisfy the conditions of photodiode or photosensor [38].

In order to obtain information concerning the photoconductivity mechanism of the diode, the relation between the short circuit current with illumination intensity is plotted on double logarithmic scale as shown in Fig. 13. The short circuit current dependence of light intensity follows the relation given by [39]:

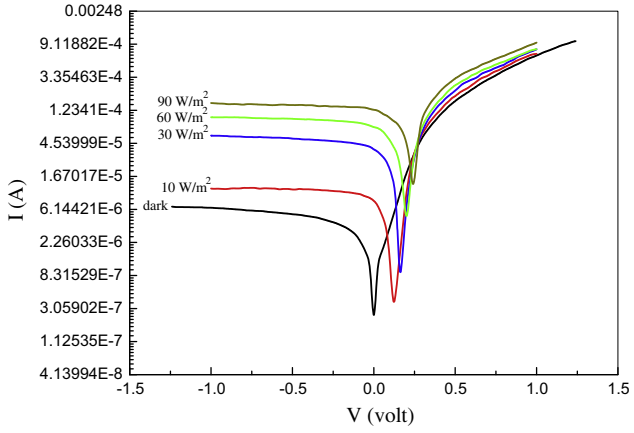

Fig. 11. Effect of illumination on the *I–V* characteristics of Au/AHNA/n-Si/Au heterojunction.

Table 1
Photovoltaic parameters of Au/AHNA/n-Si/Au heterojunction diode at various illumination intensities.

Light intensity (W/m^2)	Photovoltaic parameters		
	I_{sc} (A)	V_{oc} (V)	Photoresponsivity I_{light}/I_{dark}
10	7.99×10^{-6}	0.12	41.62
30	3.77×10^{-5}	0.16	196.35
60	7.39×10^{-5}	0.21	384.90
90	1.25×10^{-4}	0.245	651.04

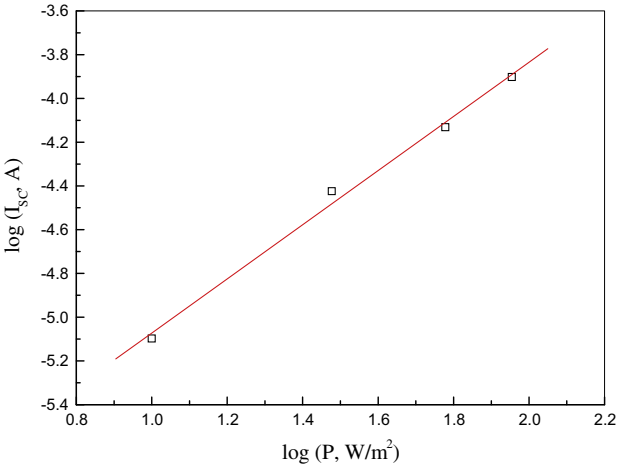

Fig. 13. Double logarithmic plot of I_{sc} versus light intensity.

$$I_{sc} = BP^{\gamma} \quad (16)$$

where B is a constant, P is the intensity of light and γ is its exponent. The γ values are 0.5 and 1.0 for bimolecular recombination and monomolecular recombination mechanisms, respectively. The obtained γ value for Au/AHNA/n-Si/Au diode is estimated as 1.22 indicating that the photoconductivity mechanism is controlled by monomolecular recombination [40].

Summary and conclusions

AHNA thin films were deposited by thermal evaporation onto glass and n-type Si substrate. The optical properties of AHNA film have been studied in the spectral range 190–2500 nm in which

the absorption coefficient and refractive index are calculated. The indirect allowed transition of the film was observed with band gap of 3.6 eV. Urbach's energy is determined as 0.48 eV. The refractive index showed normal dispersion over the spectral range 560–2500 nm and the dispersion energy, oscillator energy and dielectric constant at high frequency are estimated as 8.57 eV, 4.22 eV and 3.03, respectively. The electrical and photoelectrical properties of the Au/AHNA/n-Si/Au heterojunction diode have been investigated by using current–voltage characteristics. At low forward voltage, the thermionic theory is applied in which the ideality factor and the barrier height are determined as 2.62 and 0.74 eV, respectively. By using Nord's function, the series resistance and barrier height are determined as 415 Ω and 0.77 eV, respectively. At relatively high applied voltage, the device is controlled by the series resistance effect and the space charge limited current dominated by single trap of distribution is the operating conduction mechanisms. At reverse direction, the conduction is due to Poole–Frenkel and Schottky mechanisms at low and higher voltage, respectively. Under illumination, the device showed photovoltaic properties. The obtained results proved that the Au/AHNA/n-Si/Au diode can be used as a photodiode or photosensor in optoelectronic applications.

References

[1] S. Tong, D. Yuan, L. Yi, Spectrochim. Acta Part A 130 (2014) 280.
[2] E. Gondek, J. Nizioł, A. Danel, P. Szlachcic, K. Pluciński, J. Sanetra, I.V. Kityk, Spectrochim. Acta Part A 75 (2010) 1501.
[3] K. Sidler, N.V. Cvetkovic, V. Savu, D. Tsamados, A.M. Ionescu, J. Brugger, Sens. Actuat. A: Phys. 162 (2010) 155.
[4] B. Gunduz, F. Yakuphanoglu, Sens. Actuat. A: Phys. 178 (2012) 141.
[5] H. Dinçalp, O. Çimen, T. Ameri, C.J. Brabec, S. Içli, Spectrochim. Acta Part A 128 (2014) 197.
[6] E.M. Abdou, H.S. Hafez, E. Bakir, M.S.A. Abdel-Mottaleb, Spectrochim. Acta Part A 115 (2013) 202.
[7] Ö. Güllü, T. Kilicoglu, A. Türüt, J. Phys. Chem. Solids 71 (2010) 351.
[8] S. Concilio, V. Bugatti, H.C. Neitzert, G. Landi, A.D. Sio, J. Parisi, S. Piotto, P. Iannelli, Thin Solid Films 556 (2014) 419.
[9] F. Yakuphanoglu, M. Kandaz, B.F. Senkal, Sens. Actuat. A: Phys. 153 (2009) 191.
[10] F. Yakuphanoglu, W.A. Farooq, Synth. Met. 161 (2011) 324.
[11] K. Rafikova, N. Kystaubayeva, M. Aydemir, C. Kayan, Y.S. Ocak, H. Temel, A. Zazybin, N. Gürbüz, I. Özdemir, J. Organometallic Chem. 758 (2014) 1.
[12] E.M. El-Menyawy, A.M. Mansour, N.A. El-Ghamaz, S.A. El-Khodary, Physica B 413 (2013) 31.
[13] E.M. El-Menyawy, H.M. Zeyada, M.M. El-Nahass, Solid State Sci. 12 (2010) 2182.
[14] H.M. Zeyada, M.M. El-Nahass, E.M. El-Menyawy, Sol. Energy Mater. Sol. Cells 92 (2008) 1586.
[15] H.M. Zeyada, M.M. El-Nahass, I.K. El-Zawawi, E.M. El-Menyawy, Eur. Phys. J. Appl. Phys. 49 (2010) 10301.
[16] M.M. El-Nahass, M.A. Kamel, E.M. El-Menyawy, Spectrochim. Acta Part A 79 (2011) 618.
[17] E.M. El-Menyawy, J. Mol. Struct. 1068 (2014) 198.
[18] E.M. El-Menyawy, I.T. Zedan, H.H. Nawar, Physica B 437 (2014) 58.
[19] E.M. El-Menyawy, A.A. Elagamey, S.R. Elgogary, R.A.N. Abu El-Enein, Spectrochim. Acta Part A 108 (2013) 75.
[20] E.M. El-Menyawy, A.A. Elagamey, S.R. Elgogary, R.A.N. Abu El-Enein, Mater. Sci. Semiconductor Process. 16 (2013) 1828.
[21] J. Tauc, A.J. Menth, Non-Cryst. Solids 8–10 (1972) 569.
[22] F. Urbach, Phys. Rev. 92 (1953) 1324.
[23] M.M. El-Nahass, S. Yaghmour, Appl. Surf. Sci. 255 (2008) 1631.
[24] A. Stendal, U. Beckars, S. Wilbrand, O. Stenzel, C. Von Borczys-kowski, J. Phys. B: At. Mol. Opt. Phys. 29 (1996) 2589.
[25] S.H. Wemple, M. DiDomenico, Phys. Rev. B3 (1970) 1338.
[26] S.M. Sze, Physics of Semiconductor Devices, John Wiley & Sons, New York, 1981.
[27] S.S. Li, Semiconductor Physical Electronics, Springer, USA, 2006.
[28] A. Bengi, U. Aydemir, S. Altındal, Y. Ozen, S. Ozcelik, J. Alloys Compd. 505 (2010) 628.
[29] P. Durmuş, M. Yıldırım, Mater. Sci. Semiconductor Process. 27 (2014) 145.
[30] Ö.T. Özmen, E. Yağlıoğlu, Mater. Sci. Semiconductor Process. 26 (2014) 448.
[31] F. Yakuphanoglu, Microelectron. Eng. 87 (2010) 1884.
[32] Ş. Altındal, T. Tunç, H. Tecimer, İ. Yücedağ, Mater. Sci. Semiconductor Process. (2014) (Article in press).
[33] H. Norde, J. Appl. Phys. 50 (1979) 5052.
[34] M.E. Aydın, A. Türüt, Microelectron. Eng. 84 (2007) 2875.
[35] F. Yakuphanoglu, N. Tugluoglu, S. Karadeniz, Physica B 392 (2007) 188.
[36] A. Ashery, A.A.M. Farag, R. Mahani, Microelectron. Eng. 87 (2010) 2218.
[37] R.D. Gould, C.J. Bowler, Thin Solid Films 164 (1988) 281.
[38] F. Yakuphanoglu, Synth. Met. 160 (2010) 1551.
[39] F. Yakuphanoglu, Sens. Actuat. A: Phys. 141 (2008) 383.
[40] R.H. Bube, Photoconductivity of Solids, Wiley, New York, 1960.